

# A *Suzaku* Search for Dark Matter Emission Lines in the X-ray Brightest Galaxy Clusters

O. Urban<sup>1,2,3\*</sup>, N. Werner<sup>1,2</sup>, S. W. Allen<sup>1,2,3</sup>, A. Simionescu<sup>4</sup>,  
J. S. Kaastra<sup>5</sup>, L. E. Strigari<sup>6</sup>

<sup>1</sup>Kavli Institute for Particle Astrophysics and Cosmology, Stanford University, 452 Lomita Mall, Stanford, CA 94305-4085, USA

<sup>2</sup>Department of Physics, Stanford University, 382 Via Pueblo Mall, Stanford, CA 94305-4060, USA

<sup>3</sup>SLAC National Accelerator Laboratory, 2575 Sand Hill Road, Menlo Park, CA 94025, USA

<sup>4</sup>Institute of Space and Astronautical Science (ISAS), JAXA, 3-1-1 Yoshinodai, Sagami-hara, Kanagawa, 252-5210 Japan

<sup>5</sup>SRON Netherlands Institute for Space Research, Sorbonnelaan 2, 3584 CA Utrecht, The Netherlands

<sup>6</sup>Mitchell Institute for Fundamental Physics and Astronomy, Texas A & M University, College Station, TX 77843-4242

November 4, 2014

## ABSTRACT

In light of recent claims of the discovery of an unidentified emission line at  $\sim 3.55$  keV in stacked *XMM-Newton* spectra for galaxy clusters, as well as *XMM-Newton* and *Chandra* spectra for the Milky Way and M31, and the possible association of this line with a decaying dark matter (DM - possibly sterile neutrino) origin, we search for the presence of unidentified emission lines in deep *Suzaku* X-ray spectra for the central regions of the four X-ray brightest galaxy clusters: Perseus, Coma, Virgo and Ophiuchus. We employ an optimized energy range for our analysis (3.2 – 5.3 keV) that is relatively free of instrumental features, and a baseline plasma emission model that incorporates the abundances of elements with the strongest expected emission lines at these energies (S, Ar, Ca) as free parameters. For the Perseus Cluster core, employing our baseline plasma model, we find evidence for an additional emission feature at an energy  $E = 3.51^{+0.02}_{-0.01}$  keV with a flux of  $2.87^{+0.33}_{-0.38} \times 10^{-7} \text{ ph s}^{-1} \text{ cm}^{-2} \text{ arcmin}^{-2}$ . At slightly larger radii, we detect an emission line at  $3.59 \pm 0.02$  keV with a flux of  $4.8^{+1.7}_{-1.4} \times 10^{-8} \text{ ph s}^{-1} \text{ cm}^{-2} \text{ arcmin}^{-2}$ . The energies and fluxes of these features are broadly consistent with previous claims, although the radial variation of the line strength appears in tension with standard dark matter model predictions. Assuming a decaying DM origin for the Perseus emission features allows us to predict the energies and detected line fluxes for the other clusters in our sample. Critically, we do not detect an emission feature at the predicted energy and line flux in the Coma, Virgo and Ophiuchus clusters. The formal 99.5 per cent upper limits on the strengths of an emission line in each cluster are below the decaying DM model predictions, scaling from the Perseus Cluster center, apparently ruling the model out. In the light of these results, which disfavor a decaying DM interpretation, we search for other explanations for the  $\sim 3.55$  keV emission feature in Perseus. Refitting the spectra with a more complex plasma model that allows the abundances of additional elements (Cl, K, Ti and V) to be free parameters removes the need for any unidentified line in the 3.5 – 3.6 keV region. Our results suggest that systematic effects associated with modeling the complex projected spectra for the Perseus Cluster core, details of the assumed ionization balance, and errors in the predicted emissivities of individual spectral lines may in part be responsible for the  $\sim 3.5$  keV feature. The upcoming *Astro-H* satellite will allow us to explore the origins of this feature more robustly.

**Key words:** dark matter, line: identification, neutrinos

## 1 INTRODUCTION

Recent claims of the discovery of a previously unknown X-ray emission line at  $\sim 3.5$  keV in the spectra of galaxy clusters (Bul-

\* E-mail: ondrej@stanford.edu

bul et al. 2014a, hereafter Bu14) and nearby galaxies (Boyarsky et al. 2014c, hereafter Bo14) have sparked a lively discussion in the community. These authors put forward the possibility that the line originates from the decay of  $\sim 7$  keV sterile neutrino dark matter (DM) particles in the halos of the observed structures.

Bu14 found a weak unidentified line at  $E = (3.55 - 3.57) \pm 0.03$  keV at a  $> 4\sigma$  significance using stacked *XMM-Newton* observations of 73 low redshift ( $0.01 < z < 0.35$ ) clusters of galaxies. The line was also seen in subsets of their sample. The authors predicted the intensity of nearby weak elemental lines based on the strong lines in their fitting band, including systematic uncertainties, and claimed that the unidentified line cannot have an astrophysical origin. Using *Chandra* observations, the authors also detected the line in the Perseus Cluster, although they made no detection in the Virgo Cluster.

Bo14 reported a  $4.4\sigma$  detection of an unidentified line at  $3.518^{+0.019}_{-0.022}$  keV in combined *XMM-Newton* observations of M31 and the Perseus Cluster. For the Perseus data, the authors measured the surface brightness profile of the feature, finding that it has a shallower slope than predicted by a  $\beta$ -model (which approximately describes the surface brightness of the intracluster medium, hereafter ICM). They claim that the radial variation of the line is consistent with a projected Navarro, Frenk & White (NFW, Navarro et al. 1996) profile.

Recently, Boyarsky et al. (2014a) also claimed a detection of a line at  $3.539 \pm 0.011$  keV in *XMM-Newton* observations of the Galactic Center. However, in this case they could not rule out an astrophysical origin for the line.

Several other studies have been published recently that challenge the presence of the line and/or the decaying DM interpretation: Using *Chandra* observations of the Milky Way, Riemer-Sorensen (2014) claim to exclude the presence of a DM emission at  $\sim 3.5$  keV at 95% confidence level. Instead, they argue, that the spectrum can be modeled using only continuum emission and known elemental lines. Jeltema & Profumo (2014) analyzed stacked *XMM-Newton* observations of the Milky Way center. They argue, that all spectral features in the  $\sim 3.5$  keV region can be explained using standard astrophysical lines, in particular those of K XVIII. Evidence for the line was also reevaluated for the Perseus observations analyzed in Bu14; after including the previously unaccounted for Cl XVII line at 3.51 keV, Jeltema & Profumo (2014) found no evidence for an unidentified line in this observation. These authors also reanalyzed the M31 observations of Bo14, finding no significant evidence for the presence of the line. Boyarsky et al. (2014b) have recently challenged this last claim, arguing that the limited 3 – 4 keV energy band used by Jeltema & Profumo (2014) may lead to biased results. Specifically, they claim that the best-fit continuum model obtained in this relatively narrow energy band overpredicts the flux observed at higher energies, between 4–8 keV. It has also been suggested by Bulbul et al. (2014b) that the analysis of Jeltema & Profumo (2014) may have been compromised by the use of erroneous values for certain line emissivities.

Malyshev et al. (2014) used stacked *XMM-Newton* observations of dwarf spheroidal galaxies to exclude the Bu14 line at  $3.3\sigma$ . Due to their large mass-to-light ratio and the fact that their interstellar medium does not produce thermal X-ray radiation, these objects provide an interesting tool for such tests. However, to conclusively exclude a DM line origin, the authors call for additional observations that would increase the sensitivity by a factor of  $\sim 2$ .

Finally, Anderson et al. (2014) analyzed observations of 81 *Chandra* and 89 *XMM-Newton* galaxies, respectively stacked in a way where each X-ray event is weighed according to the assumed

**Table 1.** List of observations used in the analysis. The columns show, respectively, the *Suzaku* observation ID, the date of the observation and the clean exposure time. The total exposure time for the Perseus Cluster is 740 ks.

Obs. ID	Obs. date	Exposure (ks)
Perseus		
800010010 <sup>†</sup>	2006-02-01	44
101012010 <sup>†</sup>	2006-08-29	46
101012020	2007-02-05	40
102011010	2007-08-15	36
102012010	2008-02-07	36
103004010	2008-08-13	41
103004020	2009-02-11	46
104018010	2009-08-26	35
104019010	2010-02-01	34
105009010	2010-08-09	30
105009020	2011-02-03	33
105010010	2010-08-10	25
105027010	2011-02-22	42
106005010	2011-07-27	34
106005020	2012-02-07	42
106006010	2011-07-26	33
107005010	2012-08-20	34
107005020	2013-02-11	36
108005010	2013-08-15	38
108005020	2014-02-05	34
Coma		
801097010 <sup>†</sup>	2006-05-31	164
Virgo		
801038010	2006-11-29	90
Ophiuchus		
802046010	2007-09-24	83

<sup>†</sup> observations with available XIS2 exposure

DM profile in its respective galaxy. The authors ruled out the presence of the purported DM decay line at  $4.4\sigma$  and  $11.8\sigma$  confidence in the *Chandra* and *XMM-Newton* samples, respectively.

A brief review of the current status of the observational results and theoretical interpretations of the  $\sim 3.5$  keV feature, including implications for dark matter small-scale structure (Abazajian 2014), can be found in Iakubovskiy (2014).

In this paper, we present our own search for unidentified emission lines in *Suzaku* observations of the four X-ray brightest galaxy clusters: Perseus, Ophiuchus, Virgo and Coma (Edge et al. 1990) – all of which have relatively long exposures. Additionally, unlike the previous works, we fit all spectra in parallel, avoiding stacking and the complications it brings. In particular, systematic effects, due to the smearing of spectral features by e.g. gain variations, are reduced in our analysis.

Sect. 2 of this paper describes our data analysis and modeling approach. In Sect. 3 we present the main results from our analysis and in Sect. 4 we discuss their implications. Our conclusions are summarized in Sect. 5. Throughout this paper, all errors are quoted at 68 per cent level of confidence and all line energies are quoted and plotted in the rest frame, unless stated otherwise.

## 2 OBSERVATIONS AND DATA ANALYSIS

The details of the *Suzaku* observations utilized in this study are shown in Tab. 1. For each cluster, we analyzed data from all X-ray Imaging Spectrometers (XIS 0, 1, 2 and 3) obtained in the normal clocking mode. XIS 2 was lost to a putative micrometeoroid hit on

November 9, 2006 and therefore its data are available only for a limited fraction of our sample.

There is only one observation for each of the Coma, Virgo and Ophiuchus cluster cores. The Perseus Cluster is a *Suzaku* calibration source and as such it has been observed regularly since the launch of the satellite. We use all observations for Perseus obtained in the normal clocking mode with no window option, with a total exposure time of 740 ks.

## 2.1 Data Cleaning

Initial cleaned event lists were obtained using the standard screening criteria proposed by the XIS team<sup>1</sup>. Given the energy band used for the analysis (3.2 – 5.3 keV, see Sect. 2.3), we do not expect any significant influence from the solar wind charge-exchange (SWCX) emission, whose lines are expected below 1.5 keV (Fujimoto et al. 2007). We filtered out times of low geomagnetic cut-off rigidity ( $COR \leq 6$  GV). For the XIS 1 data obtained after the reported charge injection level increase on June 1st 2011, we have excluded two adjacent rows on either side of the charge-injected rows (the standard is to exclude one row on either side).

## 2.2 Spectral Analysis

For the Coma, Virgo and Ophiuchus clusters, we extracted spectra from the full field of view of the XIS detectors, excluding the regions associated with the detector edges. In the case of the Perseus Cluster we opt to define two extraction regions: a central, circular region with a radius of 6 arcmin (which we refer to as the ‘core’ region), and the rest of the detector, excluding the edges (which we term the ‘confining’ region). Spectra from each observation and for each detector were treated separately. We rebinned the spectra to have at least one count per bin, employing the extended C-statistic (Cash 1979; Arnaud 1996) in the fitting. We use night Earth observations to create the instrumental background spectra.

For each spectrum, we constructed an individual response matrix with a resolution of 16 eV, spanning the 2.0 – 6.5 keV energy band<sup>2</sup>. Ancillary response files were constructed for each spectrum with the task `XISSIMARFGEN`, at the resolution appropriate for the response matrices.

## 2.3 Spectral Modeling

Decay lines from decaying dark matter are expected to be relatively weak in the X-ray spectra of clusters. Therefore, we selected an energy band for our analysis that retains as much signal as possible, while minimizing sensitivity to the instrumental systematics. In detail, at energies just below  $\sim 3.2$  keV the effective area of the *Suzaku* mirrors is influenced by the presence of strong M-edges of gold (Tamura et al. 2006), while above 5.3 keV the modeling becomes sensitive to instrumental lines including the Mn- $K\alpha$  line at 5.9 keV (Tawa et al. 2008). For these reasons, we limited our analysis to the 3.2–5.3 keV band, which includes the region around  $\sim 3.5$  keV highlighted in previous works.

**Table 2.** CXB components for the individual clusters. The normalization of the power law is given in units of  $10^{-3}$  photons  $\times \frac{1}{20^2\pi}$  keV $^{-1}$  cm $^{-2}$  s $^{-2}$  arcmin $^{-2}$  at 1 keV.

	Perseus	Coma	Virgo	Ophiuchus
PL index	1.52	1.51	1.52	1.52
norm <sub>PL</sub>	1.28	1.15	1.28	1.28

We carried out our spectral modeling in `xspec` (Arnaud 1996, version 12.8). All spectra from a given extraction region were fitted simultaneously. We modeled the ICM emission as a single temperature plasma in collisional ionization equilibrium using the absorbed `VAPEC` or `VVAPEC`<sup>3</sup> models (Smith et al. 2001). The temperatures and normalizations of the individual spectra were left free and independent, which mitigates the effects of small differences in calibration between the individual detectors. The Galactic absorption was set to the average column along the line of sight inferred from the Leiden/Argentine/Bonn Survey (Kalberla et al. 2005). For each cluster the redshift was fixed to the value provided by the NASA/IPAC Extragalactic Database (NED). We adopted the solar abundance table of Feldman (1992). In contrast with previous works, where the data were modeled by a line-free continuum and individual gaussian line components, our approach utilizes all lines of a given element simultaneously.

`ATOMDB` v. 2.0.2<sup>4</sup> (Foster et al. 2012) shows that there are three heavy elements with lines with emissivities higher than  $5 \times 10^{-19}$  photons cm $^3$  s $^{-1}$  (for the appropriate plasma temperatures of the clusters) in the observed energy band: S, Ar and Ca. The abundances of these elements were included as free parameters in the fits. The abundances of other elements were initially fixed to 0.5 Solar, with the exception of H and He, whose abundances were set to unity.

The cosmic X-ray background (CXB) due to the unresolved point sources has been modeled with an absorbed power law (PL) component (e.g., De Luca & Molendi 2004). Other standard components of the CXB, e.g. the Galactic halo emission (Kuntz & Snowden 2000) and the emission from the local hot bubble (Sidher et al. 1996) do not significantly contribute to the observed signal in the energy band of the fit. The parameters for the CXB power law component have been fixed to the published values of Urban et al. (2014) for Perseus and Simionescu et al. (2013) for Coma, and are shown in Tab. 2<sup>5</sup>. The values for Perseus and Coma are consistent with each other within their systematic uncertainties. Assuming uniformity of the power law component across the sky, we used the Perseus values to describe the local CXB of the Virgo and Ophiuchus clusters.

## 3 RESULTS

### 3.1 Modeling With No Additional Line Component

In the first step of the analysis, we applied our baseline plasma model, including features due to S, Ar and Ca, with no additional

<sup>1</sup> Aida, M., XIS Data Analysis, <http://heasarc.gsfc.nasa.gov/docs/suzaku/analysis/abc/node9.html>

<sup>2</sup> These rebinned matrices require  $\sim 50$  times less disk space and significantly improve the speed of the analysis with respect to the default choice of 2 eV resolution and the full 0.2 – 16.0 keV *Suzaku* energy band, without compromising the accuracy of the results

<sup>3</sup> The models differ only in the number of elemental abundances they allow to fit for independently; 14 and 30 for `VAPEC` and `VVAPEC`, respectively.

<sup>4</sup> <http://www.atomdb.org/>

<sup>5</sup> No scaling of the normalization was required here. The ancillary response files in all the mentioned analyses were created using the standard assumption, utilized in the *Suzaku* analysis, of uniform emission from a circular source with a radius of 20 arcmin.

**Table 3.** Best-fit parameters for the individual extraction regions using the baseline plasma model, with no additional features (see Sect. 2.3). 60 individual spectra were modeled for both the core and the confining regions of the Perseus Cluster, with results are shown in Fig. 1. Normalizations are in the units of  $\int n_e n_H dV \times \frac{10^{-14}}{4\pi[D_A(1+z)]^2} \frac{1}{20^2\pi} \text{ cm}^{-5} \text{ arcmin}^{-2}$ .

		Perseus (core)	Perseus (confining)	Coma	Virgo	Ophiuchus
<b>kT (keV)</b>	XIS0	see Fig. 1		$8.07 \pm 0.17$	$2.61 \pm 0.04$	$9.66 \pm 0.25$
	XIS1			$8.00 \pm 0.17$	$2.61 \pm 0.04$	$9.80 \pm 0.25$
	XIS2			$8.38 \pm 0.17$	N/A	
	XIS3			$8.60^{+0.29}_{-0.18}$	$2.59 \pm 0.04$	$9.66 \pm 0.25$
<b>abundance (Z/Z<sub>⊙</sub>)</b>	S	$2.12 \pm 0.21$	$2.24 \pm 0.63$	$2.1 \pm 1.4$	$1.18 \pm 0.38$	$9.6 \pm 2.0$
	Ar	$0.43 \pm 0.03$	$0.36 \pm 0.09$	$0.58 \pm 0.20$	$0.42 \pm 0.06$	$-0.24 \pm 0.26$
	Ca	$0.65 \pm 0.01$	$0.44 \pm 0.04$	$0.38 \pm 0.09$	$0.85 \pm 0.04$	$0.68 \pm 0.11$
<b>normalization</b>	XIS0	see Fig. 1		$0.65 \pm 0.01$	$1.18 \pm 0.02$	$1.63 \pm 0.02$
	XIS1			$0.67 \pm 0.01$	$1.23 \pm 0.03$	$1.68 \pm 0.02$
	XIS2			$0.65 \pm 0.01$	N/A	
	XIS3			$0.64 \pm 0.01$	$1.28 \pm 0.03$	$1.68 \pm 0.02$
<b>C-statistic/d.o.f.</b>		34281.27/34078	33612.86/33874	2402.42/2289	1742.82/1716	1694.60/1716
<b><math>\chi^2</math>/d.o.f.</b>		34566.72/33808	28429.36/28653	2414.91/2289	1755.67/1716	1703.69/1716

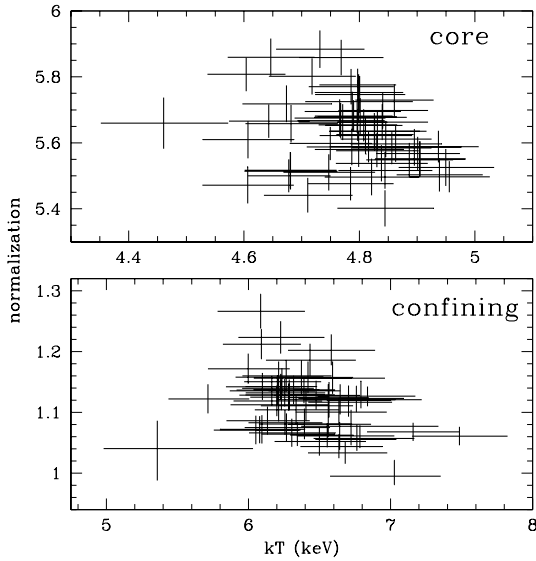


**Figure 1.** Temperatures and normalizations for the Perseus Cluster measured in the different ObsIDs and with different XIS detectors. Top panel shows the values for the core region ( $r < 6 \text{ arcmin}$ ) and the bottom panel for the confining region ( $r > 6 \text{ arcmin}$ ). The normalizations are given in the units introduced in Tab. 3.

lines. The results are summarized in Tab. 3 and Fig. 1. To estimate the goodness of fit for these baseline models, we rebinned the spectra to have at least 50 counts per bin and determined the reduced  $\chi^2$ , which are summarized in the bottom row of Tab. 3.<sup>6</sup> We ob-

<sup>6</sup> In most cases, the rebinning did not have any effect, since the Suzaku observations of bright cluster cores already contain at least 50 counts per bin. This is demonstrated by the unchanged number of degrees of freedom (d.o.f.) between the C-statistic and  $\chi^2$  fits for the longest individual observations (Coma, Virgo, Ophiuchus).

tained broadly (though in some cases not formally) acceptable values of  $\chi^2$ /d.o.f. between 0.99 (the confining region of Perseus, and Ophiuchus) and 1.06 (Coma), indicating that our baseline models describe the data reasonably well.

The temperatures measured in the individual cluster regions with the baseline models are in good general agreement with values found in literature (e.g., Fabian et al. 2011; Sanders et al. 2013; Million et al. 2010b,a, for Perseus, Coma, Virgo and Ophiuchus, respectively). Our relatively narrow fitting band does not allow us to assess the multitemperature structure present in the cluster cores. We attempted to fit the spectra with two temperature models, with the temperature of one of the components fixed first at 90 and later at 50 per cent of the value of the other. In neither case were we able to robustly constrain the contribution of the individual components to the total emission. Multitemperature structure of the cluster cores has been studied extensively in previous work on Perseus (e.g., Sanders & Fabian 2007) and Virgo (Werner et al. 2010). It is clear, therefore, that our continuum model must be biased to some degree, which must influence the predicted plasma model line strengths. This is discussed in more detail in Sect. 3.2.4 and 4.1.

Our initial fits with the baseline plasma model measured high, supersolar abundances of S, particularly in Ophiuchus and Perseus. In the former case, the high S abundance appears to compensate in part for negative residuals at the expected energies of some Ar lines, since the lines from the ions of both elements, in particular Ar xviii and S xvi, overlap in a relatively narrow energy band (between 3.27 – 3.44 keV). The high S abundance found in Perseus could also be affected by other chemical elements with weak lines. This is discussed further in Sect. 3.2.4.

### 3.2 Modeling With An Additional Line Component

To test for the presence of a spectral line in addition to the baseline model within our energy band, we added a redshifted gaussian component into the model and performed a sequence of fits for each cluster (including both extraction regions of Perseus), successively fixing the energy of this line component to values spanning the range 3.25 – 5.25 keV (in intervals of 25 eV). We allowed

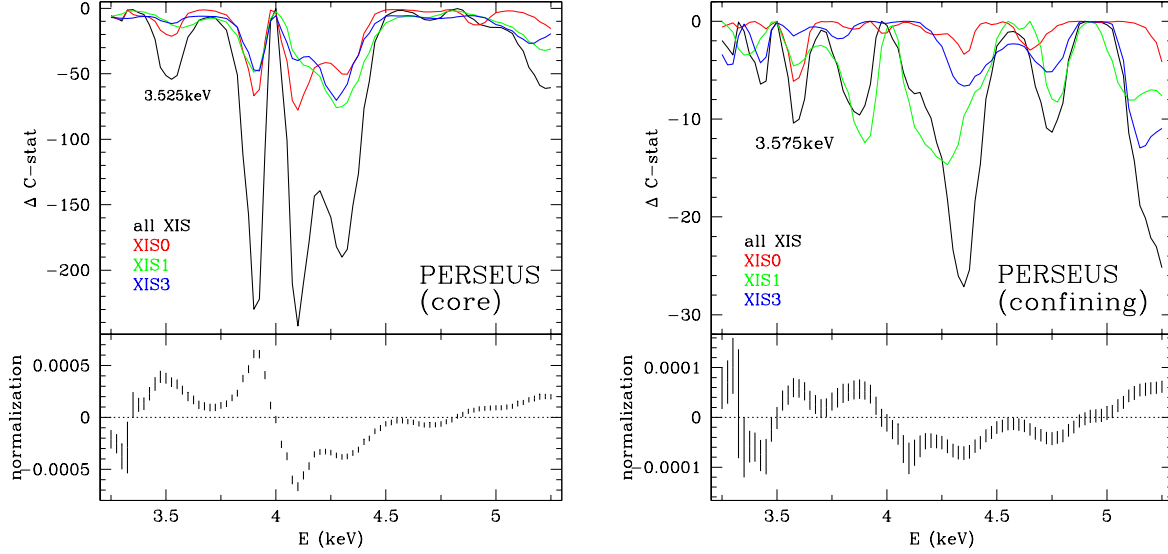


**Figure 2.** Improvement of the fit for one additional degree of freedom (the line normalization) as a function of the *rest-frame* line energy for the core (*left*) and the confining (*right*) regions of the Perseus Cluster. The top panels show the change in the C-statistic value between the models with and without the additional line component. Black lines show the results when simultaneously using the data from all the detectors and colored lines (red, green, orange, blue) using the data from the individual detectors. Bottom panels show the best-fit value for the line normalization in units of  $\frac{1}{20^2 \pi}$  photons cm<sup>-2</sup> s<sup>-1</sup> arcmin<sup>-2</sup> using the data from all detectors. Note the different scales of the vertical axes. Note also the presence of formal requirements for both emission (positive residuals) and absorption (negative residuals) features in the fits at different energies.

for both positive and negative line normalizations, and measured the improvement ( $\Delta C$ ) of the fit as a function of the line energy. In all cases we assume that the line has zero intrinsic velocity width (meaning that the width of the line in the spectral fit is set by the spectral resolution of the Suzaku detectors).

For each cluster, fits were performed on both a combined data set (fitting the data for all detectors simultaneously) and the data for the separate XIS detectors individually. The results are shown in Figs. 2 and 3.

In the rest of this section, we focus our discussion on the presence of a possible emission feature at  $E \sim 3.55$  keV, highlighted in previous works (see Sect. 1). A discussion of the other, and in some case formally more significant features, can be found in Sect. 4.3.

### 3.2.1 3.55 keV features in the Perseus Cluster

The most prominent improvement to the baseline model with the introduction of an additional line at energies around 3.55 keV is found in the data for the Perseus Cluster core region, shown in the left panel of Fig. 2. We measure  $\Delta C = -54.82$ , with respect to the baseline model, with the introduction of a line at 3.525 keV. Performing a separate fit with the line energy included as a free parameter but constrained to be in the range 3.4–3.6 keV, we find  $E = 3.510^{+0.023}_{-0.008}$  keV and a flux of  $2.87^{+0.33}_{-0.38} \times 10^{-7}$  ph s<sup>-1</sup> cm<sup>-2</sup> arcmin<sup>-2</sup> ( $\Delta C = -55.36$  for two additional d.o.f with respect to the baseline model).

A less significant feature, at  $E = 3.575$  keV, is found in the confining region of Perseus, plotted in the right panel of Fig. 2 ( $\Delta C = -10.41$ ). Including the line energy as a free parameter, we measure a line energy  $E = 3.592^{+0.021}_{-0.024}$  keV and flux  $4.78^{+1.65}_{-1.41} \times 10^{-8}$  ph s<sup>-1</sup> cm<sup>-2</sup> arcmin<sup>-2</sup> ( $\Delta C = -10.93$  for two additional d.o.f).

The energies of the lines in the core and confining regions are formally separated by more than  $3 \sigma$ . Given that tests based on the

observed energy of the Fe-K line at 6.7 keV indicate the gain to be stable within  $\sim 5$  eV during the Perseus observations, this separation is significant. Nonetheless, the 82 eV difference is smaller than the resolution of the *Suzaku* CCD detectors ( $\sim 150$  eV).

In the following argument, we adopt the assumption that these two lines have the same origin. In Sect. 3.2.3 we show, that assuming a DM decay origin of these lines, and an NFW profile for the DM density, we would expect the dark matter lines from the core and confining regions of Perseus to be comparable in strength, which is in tension with our results. Using the best-fit energies of the respective lines, they differ in fluxes by a factor of 6. This difference increases to a factor of  $\sim 14$ , when the energy of the line in the confining region is fixed to 3.51 keV (the best fit value in the core). On the other hand, when we fix the energy of the line in the core to 3.592 keV (the best-fit energy from the confining region) the difference in fluxes slightly decreases to a factor of  $\sim 4$ .

### 3.2.2 Absence of the 3.55 keV features from the Coma, Virgo and Ophiuchus clusters

We found no comparably significant emission features with energies around 3.55 keV in the Suzaku data for the Coma, Virgo or Ophiuchus clusters, with formal 95 per cent confidence upper limits on the strength of any line at  $E = 3.55$  keV of  $2.65 \times 10^{-9}$  ph s<sup>-1</sup> cm<sup>-2</sup> arcmin<sup>-2</sup>,  $2 \times 10^{-8}$  ph s<sup>-1</sup> cm<sup>-2</sup> arcmin<sup>-2</sup> and  $7.06 \times 10^{-8}$  ph s<sup>-1</sup> cm<sup>-2</sup> arcmin<sup>-2</sup>, respectively. By fitting the energies of the strongest astrophysical emission lines in the Coma, Virgo and Ophiuchus clusters we determined, that gain calibration changes can shift the energies of various spectral features by at most 30 eV in either direction in energy space. Therefore, it is improbable that other features present in the spectra of the Coma, Virgo and Ophiuchus clusters beyond this range (e.g. the 3.45 keV emission feature

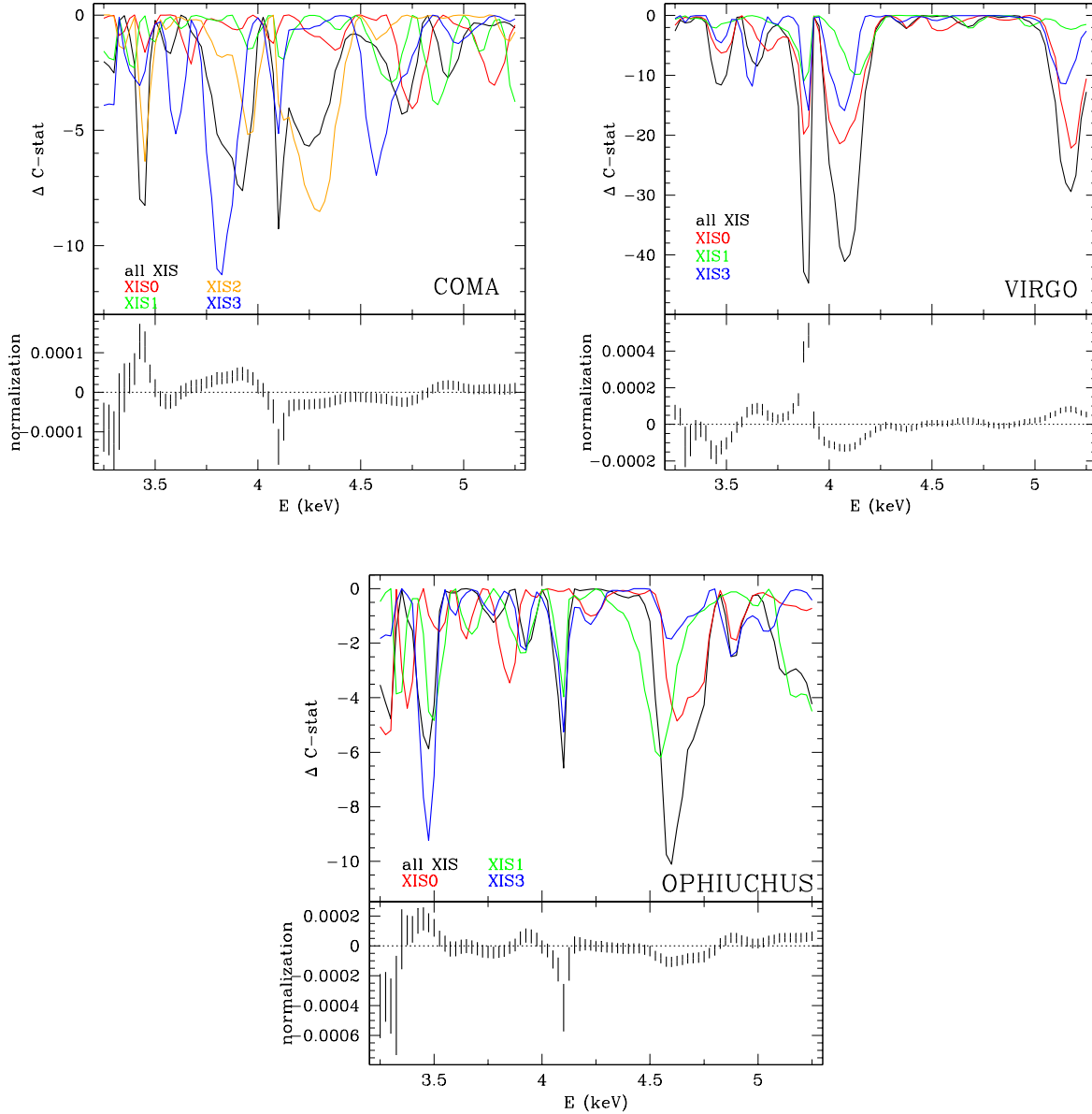


**Figure 3.** As Fig. 2 for the Coma, Virgo and Ophiuchus Clusters.

seen in the upper left panel of Fig. 3 for the Coma Cluster) has the same origin as the 3.55 keV features in the Perseus Cluster.

### 3.2.3 The 3.55 keV Line Strength Expectation

The energies and fluxes of the additional (w.r.t. the baseline plasma model; see Sect. 2.3)  $E \sim 3.55$  keV emission features detected in the Suzaku data for the Perseus Cluster core and confining region are similar to those reported by Bu14 and Bo14.

If we assume a dark matter origin for the Perseus emission features, we can predict the energies and line fluxes with which these lines should appear in the spectra for the other clusters in our sample, and test for consistency with the measured upper limits. Such a comparison provides a rigorous test of the DM hypothesis.

Assuming a decaying dark matter (e.g. sterile neutrino) origin for the Perseus emission features, the strengths of the lines in

the other clusters, relative to the Perseus core (and the confining region of Perseus), should depend only on the projected masses of dark matter within the respective spectral extraction regions, and the distances to the clusters. The three-dimensional density profiles of the dark matter halos hosting the clusters can be approximated with NFW profiles (Navarro et al. 1996):

$$\rho(r) = \frac{\delta_c \rho_c}{\frac{r}{r_s} \left(1 + \frac{r}{r_s}\right)^2}, \quad (1)$$

where  $\rho_c = \frac{3H^2(z)}{8\pi G}$  is the critical density of the Universe at redshift  $z$ , and  $r_s$  is the scale radius. We define the radius  $r_{200}$  within which the average density of the halo is  $200\rho_c$  and the concentration parameter  $c = r_{200}/r_s$ . The characteristic overdensity for the halo is

**Table 4.** Predicted scaling factors for the DM line fluxes for the individual clusters and the extraction regions. The relative normalization is the ratio of the scaling factors, shown in the third column, in a given cluster to that in the Perseus core region, which has the most significant detection of the purported line, each divided by the sizes of the respective extraction regions (e.g., a circle with a 6 arcmin radius for the Perseus core).

	$D_L$ (Mpc)	$(1+z)M_{\text{proj}}/(4\pi D_L^2)$ $(10^8 M_\odot \text{Mpc}^{-2})$	relative norm. (Perseus core)
<b>Perseus (core)</b>	77.7	7.21	
<b>Perseus (confining)</b>		7.42	0.55
<b>Coma</b>	100.7	13.8	0.67
<b>Virgo</b>	15.5	16.7	0.81
<b>Ophiuchus</b>	122.6	16.3	0.79

$$\delta_c = \frac{200}{3} \frac{c^3}{\ln(1+c) - c/(1+c)}. \quad (2)$$

Integrating Eqn. 1 along the line of sight and defining  $x = r/r_s$ , an expression for the surface density of the halo can be written<sup>7</sup> (Wright & Brainerd 2000)

$$\Sigma_{\text{NFW}}(x) = \begin{cases} \frac{2r_s\delta_c\rho_c}{(x^2-1)} \left[ 1 - \frac{2}{\sqrt{1-x^2}} \operatorname{arctanh} \sqrt{\frac{1-x}{1+x}} \right] & : x < 1 \\ \frac{2r_s\delta_c\rho_c}{3} & : x = 1 \\ \frac{2r_s\delta_c\rho_c}{(x^2-1)} \left[ 1 - \frac{2}{\sqrt{x^2-1}} \operatorname{arctanh} \sqrt{\frac{x-1}{x+1}} \right] & : x > 1 \end{cases} \quad (3)$$

Assuming the peak of the NFW profile to coincide with the peak of the X-ray emission from the given cluster, we integrate Eqn. 3 across the *Suzaku* field of view (an  $18' \times 18'$  square) for the Coma, Virgo and Ophiuchus clusters and both the core and the confining (an  $18' \times 18'$  square with a circle of 6 arcmin radius missing from the center for the latter) regions in Perseus. We assume a concentration parameter  $c = 4.1$  (Applegate et al. 2014) and the following enclosed virial masses  $M_{200} = M(r < r_{200})$ :

- $M_{200}^{\text{Perseus}} = 6.65 \times 10^{14} M_\odot$  (Simionescu et al. 2011)
- $M_{200}^{\text{Coma}} = 8.54 \times 10^{14} M_\odot$ , calculated from  $r_{200} = 70$  arcmin (Simionescu et al. 2013)
- $M_{200}^{\text{Virgo}} = 1.40 \times 10^{14} M_\odot$ , calculated from the scaling relations of Arnaud et al. (2005) for a mean temperature of 2.3 keV
- $M_{200}^{\text{Ophiuchus}} = 1.47 \times 10^{15} M_\odot$ , calculated from the scaling relations of Arnaud et al. (2005) for the clusters with  $kT > 3.5$  keV, for the mean Ophiuchus Cluster temperature of 9.4 keV.

The results of these calculations are shown in Tab. 4. The systematic uncertainties on these model predictions are probably at the tens of per cent level. To obtain the relative line normalizations w.r.t. the line normalization in the Perseus core, we used the ratios of the scaling factors (in the third column of Tab. 4), each divided by the area of the respective extraction regions in the individual clusters (e.g., a circle with a 6 arcmin radius for the Perseus core). This approach is necessary due to the definition of the normalization of *Suzaku* spectra, which is constant for an object with uniform

**Table 5.** Change of the fit with a line component, between the case when its normalization has been fixed to the expected value based on the NFW profile according to Tab. 4, and the case when it was set free. The positions of the features were fixed to their best fit values found in the core of Perseus (3.510 keV, *Core feature*) and in the confining region of Perseus (3.592 keV, *Confining region feature*), respectively. The normalization is given in the units introduced in Fig. 2. The shown difference in the C-statistic ( $\Delta C$ ) assumes a perfect knowledge of the scaling of the line strength among the individual clusters.

	line normalization		$\Delta C$
	expected	best-fit	(perfect model)
<b>Core feature</b>			
<b>Perseus (confining)</b>	1.99	$0.26 \pm 0.21$	65.52
<b>Coma</b>	2.41	$-0.04 \pm 0.21$	124.68
<b>Virgo</b>	2.92	$-0.86 \pm 0.31$	147.35
<b>Ophiuchus</b>	2.85	$1.21 \pm 0.59$	7.86
<b>total</b>			345.41
<b>Confining region feature</b>			
<b>Perseus (core)</b>	1.01	$2.30 \pm 0.43$	9.10
<b>Coma</b>	0.68	$-0.17 \pm 0.18$	19.84
<b>Virgo</b>	0.82	$0.42 \pm 0.29$	1.91
<b>Ophiuchus</b>	0.80	$-0.20 \pm 0.50$	3.97
<b>total</b>			34.82

surface brightness, irrespective of the size of the extraction region<sup>8</sup>. Therefore, since the calculations of the scaling factors in the third column of Tab. 4 depend on the extraction region, we need to “divide out” this dependence, in order to be able to directly compare the normalizations.

Given these predictions for the relative strengths of emission features due to decaying DM, we tested whether the data for our ensemble of clusters is consistent with such a model. Scaling the strength of putative 3.510 keV (3.592 keV) emission feature measured in the core (confining) region of Perseus to the Coma, Virgo and Ophiuchus clusters according to the DM model, and fixing the line strengths and energies at these predicted values, we determined new best-fit C-statistic values for the clusters. These C-statistic values were then compared with those obtained when the line strengths are left free.

The results of this test are shown in Tab. 5. We find that the scaled DM model predictions based on the Perseus core (and confining region) significantly overestimate the observed line fluxes at these energies for the other three clusters. The third column of this table summarizes the difference in C-statistic between the model with the scaled DM line and with the line strength free (assuming zero uncertainty in the DM line strength calculation). Positive numbers indicate that the fit worsens with the introduction of the DM line. Combining the results for Coma, Virgo and Ophiuchus, and the region in Perseus that the scaling was not based on, leads to a formal exclusion of the scaled 3.5 – 3.6 keV DM line model at very high significance ( $\Delta C > 340$  when scaling from the Perseus core, or  $\Delta C = 34.82$  when scaling from the confining region).

<sup>7</sup> In detail, this expression assumes that the NFW profile extends to infinity, although the differences in DM model predictions versus models truncated at the virial radii of the clusters are minimal for our extraction regions.

<sup>8</sup> For other X-ray observatories, e.g. *Chandra* or *XMM-Newton*, the normalization of such spectrum is proportional to the area of the extraction region.

As an additional test, we examined the internal self-consistency of the Perseus Cluster data, measuring the  $\Delta C$  difference between the case when the  $\sim 3.55$  line properties (the energy and normalization) were fixed at their DM predicted values, and when both the line energy and normalization were free, i.e. the case described in Sect. 3.2.1. Again, we found a large difference in the C-statistic values,  $\Delta C = 77.36$ , when fitting the confining region with a DM model scaled from the core region, and  $\Delta C = 35.41$  when fitting the core region with a DM model scaled from the confining region. Thus the radial variation of the putative DM line appears inconsistent with standard DM model expectations.

We illustrate the tension between the Perseus-scaled decaying DM model predictions and the Coma, Virgo and Ophiuchus Cluster data in Fig. 4. Here we have stacked the spectra<sup>9</sup> for the Perseus confining region and fitted the data for each cluster (over the full 3.2 – 5.3 keV band) with the baseline plasma model, also including a gaussian component at  $E = 3.510$  keV with the line strength scaled according to the decaying DM model normalized to the Perseus Cluster core. The black lines in the figure show the best-fit model when the normalization of the putative DM line is left free. The red lines show the best fit models with the 3.510 keV line normalization fixed at the predicted value for the decaying DM model, scaled from the Perseus core. In the latter case the fits are poor.

Given the large discrepancies between the DM model-predicted and measured  $\sim 3.55$  keV line strengths from all individual clusters in our sample, we conclude, that a DM decay interpretation for the origin of the  $\sim 3.55$  keV emission line can be ruled out.

### 3.2.4 Other potential origins for the 3.55keV feature: relaxing the abundances of other elements

The *Suzaku* spectra for the Perseus Cluster contain  $\sim 1.3 \times 10^7$  cumulative photons (about 85 per cent of the photons come from the core region) and are in principle deep enough to allow us to formally detect emission lines of elements other than S, Ar and Ca. This is not possible with any other data set in our sample. According to AromDB, lines of Cl, K, Ti and V with emissivities lower than  $5 \times 10^{-19}$  photons  $\text{cm}^3 \text{s}^{-1}$  are also present in our fitting band. (In detail, a total of 151 line emissivities are tabulated in our fitting band.) However, not all these lines are included in our plasma model, since the emissivities of some (predominantly weak) lines are tabulated for only a narrow range of plasma temperatures and the fitting code treats their emissivities as zero outside this range. For example, only three out of six Cl lines listed in AromDB have nonzero model emissivities at our best-fit temperatures (the remaining three lines are expected to contribute even less to the total X-ray flux). To illustrate the influence of the emission lines on the modeling, we calculated the fractional contribution of the lines of the individual elements to the emission across our fitting band, assuming a plasma temperature of 4.8 keV, Solar abundances of the individual elements, and using the *Suzaku* response files to account for the line widening. The results are shown in Fig. 5.

We performed additional fits to both extraction regions of Perseus with the abundances of the seven elements noted above set free. In the first case we included no additional (putative DM) Gaussian component in these fits. We found a significant improvement of  $\Delta C = -134.13$  and  $\Delta C = -35.91$  for four additional de-

**Table 6.** Measured abundances of all elements in the Perseus Cluster, that have lines in our fitting band (c.f. Tab 3, for the results of the modeling with only the elements with the strong lines set free). No additional Gaussian line was added to the model. All the quoted errors are statistical only.

	core	confining region
S	$0.67 \pm 0.26$	$1.28 \pm 0.73$
Cl	$15.2^{+2.3}_{-2.2}$	$7.00^{+5.54}_{-5.56}$
Ar	$0.67 \pm 0.04$	$0.43 \pm 0.12$
K	$0.95 \pm 0.44$	$0.24^{+1.17}_{-0.72}$
Ca	$0.68 \pm 0.02$	$0.45 \pm 0.05$
Ti	$2.06 \pm 0.26$	$2.02^{+0.90}_{-0.89}$
V	$12.3^{+1.5}_{-1.6}$	$35.0 \pm 5.3$

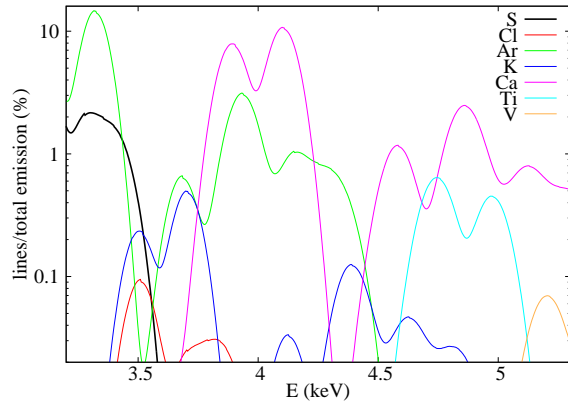


**Figure 5.** Relative contributions of the lines of the individual elements to the total emission, widened by the *Suzaku* response, for all seven elements with tabulated lines in the fitting band 3.2 – 5.3 keV. The abundances have been set to the Solar values. There are many regions where the lines overlap and, therefore, can influence each other.

grees of freedom for the core and confining regions, respectively, with respect to the baseline plasma model. The measured values of all free abundances are shown in Tab. 6.

The inferred abundances of S and Ar in the Perseus core for the model with all 7 element abundances free are significantly different than those inferred from the previous baseline analysis. This is a consequence of the complicated influence that the elemental lines have on each other due to their overlapping energies (given the limited resolution of the *Suzaku* detectors of  $\sim 150$  eV). This will be discussed further in Sect. 4.3. The abundance of S decreases with the more complex model to approximately solar (or slightly subsolar) values, from the supersolar values of, respectively, 2.12 and 2.24, measured in the baseline analysis. The abundances of all elements with strong emission lines (S, Ar, Ca) are, in the case of these 7 element fits, broadly consistent with previously reported values to the full-band spectrum (e.g., Tamura et al. 2009).

The results of our 7 element fits imply very high supersolar abundances of Cl and V. As is discussed below, and in more detail in Sect. 4, these very high abundances could in principle be artifacts caused by the multiphase structure of the gas in and around the Perseus core, as well as modeling degeneracies between the individual elemental lines (see Fig. 5) and, possibly, systematic errors in the tabulated emissivities.

<sup>9</sup> The stacking was performed using the ADDSPEC tool.



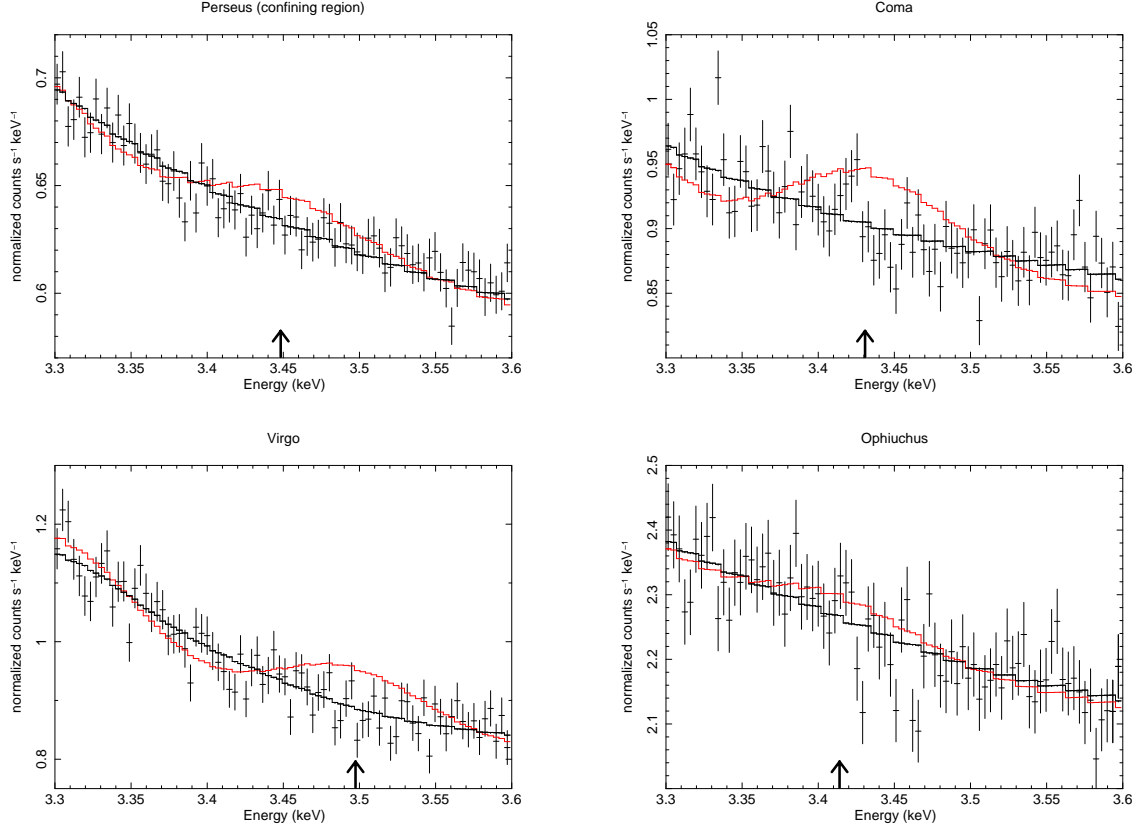


**Figure 4.** A detailed view of a narrow part of the cluster spectra in the  $\sim 3.5$  keV region plotted in the detector frame. The individual panels show the stacked spectra of the individual clusters (*points*), and the best-fit models including the gaussian line with the normalization set free (*black lines*) and fixed to the predicted value based on the assumption that the line detected in the Perseus core is due to DM decay (*red lines*), respectively. The black arrows indicates the energy of the gaussian line component in the detector frame. The fitting has been performed in the full 3.2 – 5.3 keV energy band. The stacking of the spectra has been done solely for the illustration purposes and we drew no conclusions based on the analysis of the stacked spectra. The saw-like features seen in the model lines appear due to the limited energy resolution of the response matrices (16eV) and the resulting discontinuities in the effective area.

Three (two) of the six Cl lines included in AromDB have nonzero emissivities at the best-fit temperature of the core (confining) region. These are shown in the top panel of Fig. 6. Two Cl xvii lines at 3.51 keV appear in both extraction regions, while the 3.70 keV line of the same ion appears only in the core region. The 3.51 keV line complex is of particular interest. If there is an unidentified emission line present nearby, it could blend with this complex and cause an upward bias in the Cl abundance. As a test, we removed the 3.4 – 3.6 keV band from the Perseus core spectra and refitted the data<sup>10</sup>. We obtained a marginally higher Cl abundance of  $21.7 \pm 4.3$  compared to the original case, with no evidence for extra emission around  $\sim 3.55$  keV. Performing an analogous test, while removing the 3.6–3.8 keV band, which contains the 3.70 keV Cl line, resulted in a formal value of  $25^{+2}_{-3}$  for the Cl abundance. These tests show the complicated way, in which the elemental lines are influenced by the multitemperature structure of the gas and also by the lines of other elements in the spectrum. This will be discussed in Sect. 4.3.

The only V line in our spectra lies at 5.21 keV, making the measured V abundance very sensitive to systematic effects, including those stemming from improper continuum fitting. This is sup-

ported by the fact, that, in the fit with the 3.70 keV band excluded, as described above, we observed a small increase in the average temperature to  $\sim 4.95$  keV and a decrease in V abundance to 9.8. This suggests the presence of extra emission at the high energy end of the fitting band, with respect to the model, which is modeled by a strong V line. Possible systematic effects responsible for this surplus emission are discussed in Sect. 4.3.

The formal abundances of the other two elements with weak lines, K and Ti, do not immediately look unrealistic (see Tab. 6). However, they, too, may be subject to bias. Although our results show, that formal measurements of the chemical abundances of a large set of elements are possible with current data, systematic effects make the interpretation of these results challenging.

We next performed a test for the presence of an additional line, analogous to that introduced in Sect. 3.2, but now with the abundances of all seven elements free. The results are shown in Fig. 7 with the main minima labeled and discussed in Sect. 4.3. The curves for the Perseus core in Fig. 7 and the left panel of Fig. 2 are broadly similar, except for the near disappearance of the minima at 3.525 keV and 5.225 keV and the appearance of a new minimum at 3.7 keV in Fig. 7.

The minimum previously at 3.525 keV has been reduced in depth and shifted by 25 eV, so that it now lies at 3.5 keV, and is now associated with an *absorption* feature. Given, that this change has been achieved simply by including the abundances of chemical

<sup>10</sup> It is not possible to perform this test with the data from the confining region, as it would remove all the Cl lines.

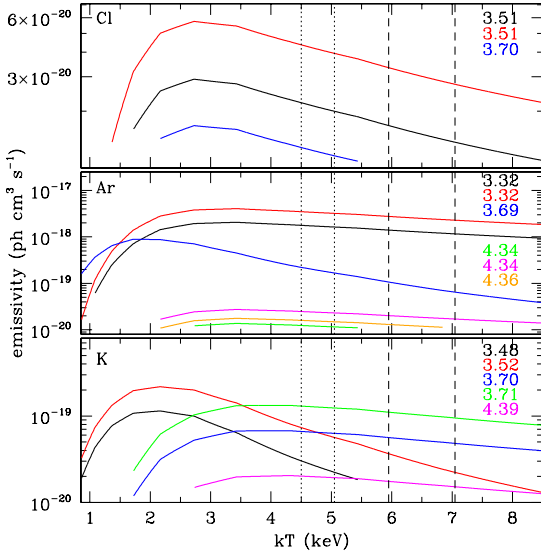


**Figure 6.** Emissivities for the lines of Cl (*top*), Ar (*middle*) and K (*bottom*) as a function of the plasma temperature. The individual line energies in keV are marked in each panel. The approximate ranges for the best-fit temperatures are marked for the Perseus core (*dotted lines*) and the confining (*dashed lines*) regions. We show the complete set of the Cl and K lines that appear in our fits, but only those emissivities of the Ar lines that are relevant to the discussion (see text).

elements with weak emission lines as additional free parameters in the modeling, an elemental origin of the feature seen in Fig. 2, as opposed to a DM emission line, cannot be excluded. Other possible reasons for the remaining presence of this minimum are discussed in Sect. 4.3.

The curve for the confining region in Perseus is changed dramatically from that in Fig. 2, and now shows only one, previously unseen, significant feature at 3.5 keV. The best-fit Gaussian at this energy again has a *negative* normalization and is accompanied by a large increase of the Cl abundance to a value of  $\sim 100$ . This effect is probably an artifact of the fitting, where the unrealistically strong lines of Cl in the model, caused by the formally high value of the abundance, are compensated for by the negative residuals from the normalization of the Gaussian line component.

## 4 DISCUSSION

In the last section we presented evidence suggesting that a previously reported emission line around 3.55 keV in the Perseus Cluster probably does not have a dark matter origin, but can instead be explained by elemental lines, given the current systematic errors in their tabulated intensities. In the following section we compare our results with those reported previously in the literature, and present further discussion of the DM hypothesis.

### 4.1 Arguments relating to the DM Interpretation of Line Emission Around 3.55 keV

In Sect. 3.2.1 we saw that, when we took into account only the chemical elements with the line emissivities higher than  $5 \times 10^{-19}$  photons  $\text{cm}^3 \text{s}^{-1}$ , we found evidence for emission lines in the

core and the confining regions of the Perseus Cluster with respective best-fit energies of  $3.510^{+0.023}_{-0.008}$  keV and  $3.592^{+0.021}_{-0.024}$  keV and fluxes of  $2.87^{+0.33}_{-0.38} \times 10^{-7} \text{ph s}^{-1} \text{cm}^{-2} \text{arcmin}^{-2}$  and  $4.78^{+1.65}_{-1.41} \times 10^{-8} \text{ph s}^{-1} \text{cm}^{-2} \text{arcmin}^{-2}$ , respectively. Although the  $82 \pm 1$  eV difference between these line energies is formally significant at the  $\sim 3\sigma$  level, it is smaller than the resolution of a *Suzaku* detector.

Both of these lines lie near the feature reported by Bu14, who found an emission line in Perseus, assuming a line energy of 3.57 keV (fixed), with a flux of  $1.22^{+0.56}_{-0.36} \times 10^{-7} \text{ph s}^{-1} \text{cm}^{-2} \text{arcmin}^{-2}$  (using a circular extraction region with the radius of 700 arcsec). Bo14 found an emission line at  $3.518^{+0.019}_{-0.022}$  keV in a combined analysis of M31 and the Perseus Cluster. However, the latter work quotes no value for the line flux.

The energies of the emission features we detect in the Perseus Cluster are formally inconsistent with the values of Bu14 and Bo14 (with the exception of the feature we found in the confining region, whose energy is consistent with the value found by Bo14). However, the difference is less than the energy resolution of the XIS detectors onboard *Suzaku* ( $\sim 150$  eV).

At face value, the fluxes of the emission features reported here and in Bu14 are also broadly consistent. The differences in the results are smaller than the systematic uncertainties in the line flux reported by Bu14 (their Tab. 5), where the fluxes of the 3.57 keV feature measured by the different *XMM-Newton* detectors differ up to a factor of a few. Moreover, the differences can in part be caused by the different energies in the reported lines. For example, when we fixed the line energy in the Perseus core at 3.57 keV (the energy used in Bu14), our measured line flux decreases by  $\sim 30$  per cent, to  $(2.08 \pm 0.34) \times 10^{-7} \text{ph s}^{-1} \text{cm}^{-2} \text{arcmin}^{-2}$ . Finally, Bu14 used different spectral extraction region from the analysis presented here, which can also introduce differences between the measured fluxes.

The arguments discussed above suggest a common origin of the  $\sim 3.55$  keV lines measured here in both extraction regions of the Perseus Cluster and those reported in Bu14 and Bo14. In this case, the line strength scaling arguments presented in Sect. 3.2.3 challenge the DM interpretation for the origin of the line. Specifically, we showed, that the line strength does not follow the expected scaling relations based on NFW modeling of the DM profiles in the Coma, Virgo and Ophiuchus clusters or indeed radially in Perseus itself. The assumption of DM origin for the 3.510 keV line, with a line strength scaled to the value measured in the Perseus Cluster core leads to an expected strength of this line that over-predicts the signal in the other clusters. The upper limits of the measured line strengths in each cluster are inconsistent with the expected line strength at more than 99.5 per cent level. The Virgo Cluster, where we observe a significantly negative normalization of the line at 3.510 keV (see Tab. 5) is particularly challenging to the dark matter interpretation. The discrepancy between the expected and measured line strengths is less pronounced but still significant when normalizing the DM model predictions to the Perseus confining region.

Formally, the tension between the expected and measured line strength for the two Perseus Cluster regions also strongly disfavours the DM origin interpretation. In Sect. 3.2.3 we showed, that we should expect the line strength from the Perseus confining region to be approximately half that in the Perseus core. However, we observe a putative DM line flux in the Perseus core that is up to  $\sim 14$  times higher than the flux from the confining region, at the same energy. In fact, due to the point-spread function (PSF) contaminating the confining region spectra with core emission to some degree (which increases the expected surface brightness of the confining

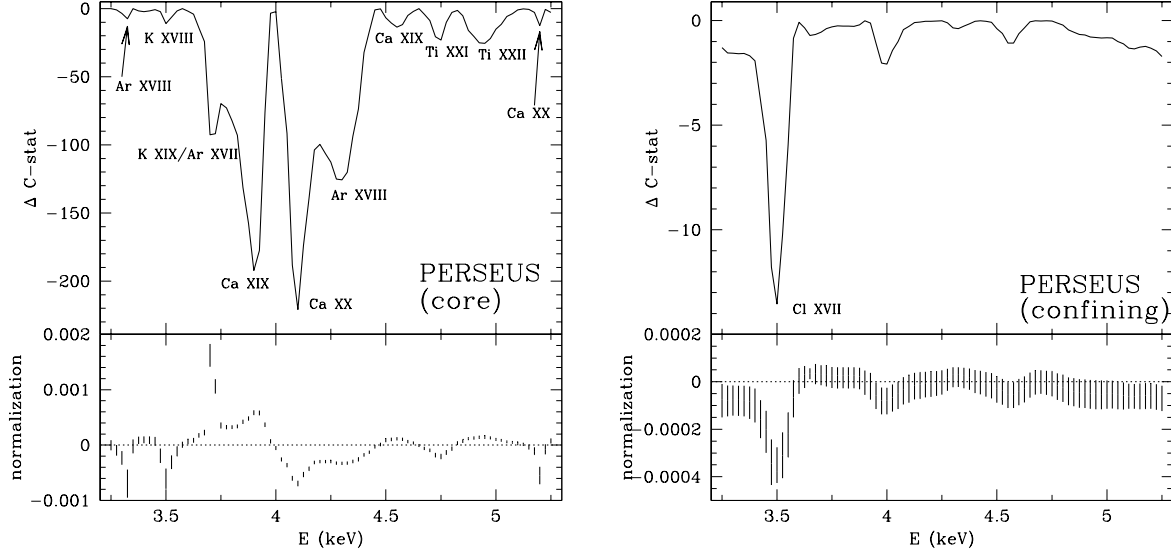


**Figure 7.** Improvement of the fit as a function of the rest frame line energy for the Perseus core (*left*) and the confining region (*right*), with seven elemental abundances (S, Cl, Ar, K, Ca, Ti, V) kept free. For the details of the labels see Sect. 4.3.

region), the actual ratio between the fluxes is probably higher, increasing the discrepancy.

Finally, including a larger set of heavy element lines in the modeling significantly reduces the requirements for the  $\sim 3.55$  keV line in Perseus.

## 4.2 Systematic Effects Influencing the Detailed Chemical Composition of the Perseus Cluster ICM

The Perseus Cluster data allow us to probe the detailed chemical composition of the ICM. *AtomDB* contains 151 tabulated lines in the fitting band of 3.2 – 5.3 keV for a total of seven chemical elements: S, Cl, Ar, K, Ca, Ti and V. We were able to formally constrain nonzero abundances for all of these elements, as shown in Tab. 6. However, as discussed in Sect. 3.2.4, the formal values of the abundances, especially for the elements with weak emission lines – Cl, K, Ti and V – are probably dominated by systematic effects. In this section we discuss potential origins for these effects in detail, including the presence of multiphase gas, overlapping line energies, systematic uncertainties in the tabulated line emissivities and artifacts of the fitting process itself.

We expect the multitemperature structure of the ICM in the Perseus core (that we cannot account for with our single temperature model) to introduce an upward bias in the measured abundances of all elements. The emissivities of all emission lines, except for the lines of Ti xxii (at 4.97 keV and 4.98 keV) and the weak lines of Ca xx with energies higher than 4.86 keV, peak at temperatures lower than the average best-fit temperature of  $\sim 4.8$  keV that we measure in the Perseus core. Therefore, these lines will appear overabundant in this region, where we know cooler gas is present (Sanders & Fabian 2007).

Due to the limited energy resolution of the *Suzaku* CCD detectors ( $\sim 150$  eV) and a relatively high number of the elemental lines in our fitting band, we observe a number of overlaps between the individual lines, which can be seen in Fig. 5. Combined with the systematic uncertainty in the tabulated emissivities of the weak, and

especially the satellite lines, which can reach  $\sim 10 - 20$  per cent, these can introduce bias to the measured abundances.

We can examine the very high formal values of the Cl abundance of  $15 \pm 2$ , reported in Sect. 3.2.4, as a potential example of these effects. In the Perseus core, Cl lines are present at 3.51 keV and 3.70 keV, and at their respective energies they contribute  $\sim 2\%$  and  $\sim 0.5\%$  to the total spectral signal, assuming the measured abundance of Cl (cf. Fig. 5 for the line contribution to the total signal at the Solar abundances). In Sect. 3.2.4 we showed, that the high Cl abundance is formally robust and not caused by a presence of an unidentified emission line blending with one of the Cl lines. (In detail, we showed that if we remove either of the energy bands containing the Cl lines (3.4 – 3.6 keV and 3.6 – 3.8 keV for the 3.51 keV and the 3.70 keV lines, respectively), the abundance does not decrease.)

The lines of three elements, Cl, Ar and K, contribute to the spectrum in the  $\sim 3.70$  keV band. The abundance of Ar is predominantly determined from the 3.32 keV lines, which constitute the strongest line complex in our spectra. Their emissivities peak at the temperature of  $\sim 3.4$  keV, while the emissivities of the Ar lines in the  $\sim 3.70$  keV band peak at lower temperatures of  $< 1.7$  keV. In the presence of relatively cool gas in the Perseus core, that our single temperature model cannot account for, the latter set of Ar lines would be underpredicted, causing surplus emission in the  $\sim 3.70$  keV energy band. [Alternatively, if there are differences between the true and the tabulated values of the emissivities of the Ar lines in the  $\sim 3.70$  keV region, specifically, if the tabulated values underestimate the true value, a surplus emission would appear at the energies around  $\sim 3.70$  keV, since the Ar abundance is well determined from the strongest lines at 3.32 keV.] The fitting code can mistakenly interpret the surplus at  $\sim 3.70$  keV as having been produced by the lines of extremely abundant Cl.

In the case of the systematic influence on the Cl lines at 3.51 keV, the scenario is more complicated. Qualitatively, the Ar lines could, in a similar fashion as discussed above, influence the measured abundances of S (overlap in the  $\sim 3.3$  keV band, see Fig. 5) and K (overlap in the  $\sim 3.7$  keV and  $\sim 4.3$  keV bands). The

lines of the two latter elements contribute to the emission in the  $\sim 3.5$  keV region and could, in turn, have an influence on the apparent Cl line strength.

We identified extra emission at the high energy end of the spectrum with respect to the model as the reason for the high formal value of V abundance in Sect. 3.2.4. This extra emission may appear due to a systematic error in the calibration of the effective area as a function of energy, which would primarily affect the edge of the fitting band and may subsequently lead to an apparent surplus of emission at the high energy end of our fitting band. Alternatively, if emission with temperature higher than  $\sim 4.8$  keV, measured in the Perseus core, was present in our spectra (e.g. in projection from the higher parts of the cluster atmosphere, or from an additional power-law spectral component), the continuum would fall off slower than predicted by our single temperature model, again leading to surplus emission at the high energy end of the spectrum. Similarly, the emission from the confining region could be contaminated by the colder emission from the cluster core due to the PSF effects (see Sect. 4.1), causing a downward bias in the best fit temperature and a quick fall off of the model spectrum with respect to the data, which would then lead to the same effect. Unfortunately, the data do not allow us to perform a multitemperature fit to test this possibility in either of these regions.

### 4.3 Spectral Signatures of the Ionization Balance and the Multitemperature Structure

Figs. 2 and 7 exhibit multiple minima for each cluster, showing formally significant improvements to the fit by adding a gaussian line component at a given energy to the model. Here we discuss possible causes for these features.

As shown in Sect. 3.2.4, some of these minima can be removed, or reduced in depth, with more sophisticated models for the abundances of elements with weak spectral lines. This was seen for the 3.525 keV and 5.225 keV features in the Perseus core and all of the minima in the Perseus confining region.

However, multiple features remain present in these data even after accounting for the elements with weak lines. Since detailed fitting was only possible with the Perseus data, and given, that the Perseus core spectra retained many of its features when fitting with three or seven free elemental abundances, we predominantly focus our discussion on the results in the left panel of Fig. 7.

The left panel of Fig. 7, for the Perseus core, is rich in features. All the minima lie at, or near, emission lines of various elements that have been labeled in the figure. We point out, that for each labeled element, a pair of ions is present, e.g. Ca xix and Ca xx. Moreover, if a given element is associated with multiple minima, the signs of the best-fit normalization of the gaussian component in the model are opposite for each ion of the pair, e.g. the minima at the position of Ca xix (xx) lines are always associated with a positive (negative) line normalization.

This suggests problems in the assumed ionization balance for the elements in the cluster core. If the ratio of different ions of the given element differs from the expected equilibrium value, its measured abundance will lie between the values that would be determined from the lines of individual ions. The additional line component in our model allows the fit to compensate for this discrepancy.

In effect, we are underestimating the abundances of Ar xvii (with a strong line at 3.69 keV), K xix (strongest line at 3.71 keV), Ca xix (with a complex of lines around 3.9 keV and another at 4.6 keV) and Ti xxii (unresolved lines at 4.97 keV and 4.98 keV), and overestimating the abundances of Ar xviii (complex of lines

at the low energy end of our fitting band with the strongest line at 3.32 keV), K xviii (complex of lines around 3.5 keV), Ca xx (complex of lines around 4.1 keV with the strongest at 4.107 keV) and Ti xxi (complex of lines around 4.75 keV).

The features in Fig. 7 could also in part be explained by the multitemperature structure of the projected emission from the Perseus core, that we are unable to model fully. In the multitemperature gas, different gas phases will contain elemental ions in different concentrations, as governed by the local temperature, and the individual ion populations will contribute to the emission lines with different strengths. Therefore, it may not be possible to assign a single temperature to the gas based on the line strengths. This was seen by Jeltema & Profumo (2014), who used the emission line strength ratios quoted by Bu14 to estimate the plasma temperature in the Perseus observations, and obtained a range of inconsistent values. However, we note, that Jeltema & Profumo (2014) were using the line strength estimates provided by the *WEBGUIDE* tool of *ATOMDB*, that can significantly differ from values obtained using the full calculation (Bulbul et al. 2014b).

The multitemperature structure of the gas in Perseus has been observed before (e.g., Sanders & Fabian 2007), which lends support to the above scenario. However, a relatively complicated temperature distribution would be required to explain the multitude of minima in Fig. 7. For instance, lower temperature gas, unaccounted for in the analysis, could cause the emission lines from ions with a lower stage of ionization to be present in higher concentration, qualitatively describing the behaviour of the Ca ions in Fig. 7. However, an opposite process seems to be influencing Ti, where the gaussian component seems to be compensating for a too high measured abundance of Ti xxi by fitting to a negative value and vice versa for Ti xxii. If this is also due to a multi-phase structure of the gas, it would suggest the additional presence of a third spectral component corresponding to a temperature that is higher than the measured average.

The example scenarios outlined in Sect. 4.2 and this section illustrate the complicated interaction between various systematic effects on the spectral modeling. To attempt to disentangle these effects is beyond the capabilities of *Suzaku*, given the limited spectral resolution. Observations with next generation detectors, especially the calorimeters onboard *Astro-H*, will be required to provide more robust constraints on the chemical composition and thermal structure of the ICM.

## 5 CONCLUSIONS

In light of the recent claims of the discovery of an unidentified emission line at  $\sim 3.55$  keV and its possible dark matter origin, we have used *Suzaku* observations to search for unaccounted emission lines in the 3.2 – 5.3 keV energy band in the spectra of the four X-ray brightest galaxy clusters. Our main conclusions are:

- Using a single temperature model with the abundances of S, Ar and Ca as free parameters, we detected emission lines at  $E = 3.51^{+0.02}_{-0.01}$  keV in the core, and  $E = 3.59 \pm 0.02$  keV in the regions surrounding the core, of the Perseus Cluster. The properties of these lines are broadly consistent with the previously reported unidentified lines in this energy band. If these lines are produced by the dark matter particle decay, they should be observed in other clusters with a strength proportional to the projected mass of the dark matter within our field of view. However, scaling from the Perseus Cluster core, we measured the upper limits of the strength of these lines in the other clusters that are in each case inconsistent

with the DM model predictions at more than 99.5 per cent level, disfavouring the DM origin hypothesis. The radial variation of the putative DM line strength in Perseus is also in apparent tension with the DM model hypothesis for the 3.55 keV line.

- Our analysis suggests that the  $\sim 3.55$  keV line features measured in the Perseus Cluster may have an elemental origin. The observations of the Perseus Cluster allowed us to formally measure the abundances of seven elements: S, Cl, Ar, K, Ca, Ti and V, with emission lines in the 3.2 – 5.3 keV energy band. Even though we obtain a significant nonzero value for the abundance for each of the seven elements, these measurements are, particularly for the elements with relatively weak emission lines (Cl, K, Ti and V), heavily influenced by systematic effects, including the presence of multitemperature structure in the Perseus Cluster; overlaps between the individual lines due to the limited resolution of the *Suzaku* detectors; systematic errors in the tabulated values of the line emissivities; uncertainties in the detector effective area calibration; and problems with the assumed ionization balance. These systematics are in big part exacerbated by the limited resolution of the CCD detectors ( $\sim 150$  eV). Next generation X-ray detectors with a  $\sim$ few eV resolution, starting with *Astro-H*, will be needed to perform more robust measurements of the chemical composition of the ICM.

## ACKNOWLEDGMENTS

This work was supported in part by the US Department of Energy under contract number DE-AC02-76SF00515. This research has made use of data obtained from the *Suzaku* satellite, a collaborative mission between the space agencies of Japan (JAXA) and the USA (NASA).

## REFERENCES

- Abazajian, K. N. 2014, Physical Review Letters, 112, 161303
- Anderson, M. E., Churazov, E., & Bregman, J. N. 2014, ArXiv e-prints: 1408.4115
- Applegate, D. E., von der Linden, A., Kelly, P. L., et al. 2014, MNRAS, 439, 48
- Arnaud, K. A. 1996, in Astronomical Society of the Pacific Conference Series, Vol. 101, Astronomical Data Analysis Software and Systems V, ed. G. H. Jacoby & J. Barnes, 17
- Arnaud, M., Pointecouteau, E., & Pratt, G. W. 2005, A&A, 441, 893
- Boyarsky, A., Franse, J., Iakubovskyi, D., & Ruchayskiy, O. 2014a, ArXiv e-prints: 1408.2503
- Boyarsky, A., Franse, J., Iakubovskyi, D., & Ruchayskiy, O. 2014b, ArXiv e-prints: 1408.4388
- Boyarsky, A., Ruchayskiy, O., Iakubovskyi, D., & Franse, J. 2014c, ArXiv e-prints: 1402.4119
- Bulbul, E., Markevitch, M., Foster, A., et al. 2014a, ApJ, 789, 13
- Bulbul, E., Markevitch, M., Foster, A. R., et al. 2014b, ArXiv e-prints: 1409.4143
- Cash, W. 1979, ApJ, 228, 939
- De Luca, A. & Molendi, S. 2004, A&A, 419, 837
- Edge, A. C., Stewart, G. C., Fabian, A. C., & Arnaud, K. A. 1990, MNRAS, 245, 559
- Fabian, A. C., Sanders, J. S., Allen, S. W., et al. 2011, MNRAS, 418, 2154
- Feldman, U. 1992, Physica Scripta, 46, 202
- Foster, A. R., Ji, L., Smith, R. K., & Brickhouse, N. S. 2012, ApJ, 756, 128
- Fujimoto, R., Mitsuda, K., Mccammon, D., et al. 2007, PASJ, 59, 133
- Iakubovskyi, D. 2014, ArXiv e-prints: 1410.2852
- Jeltema, T. E. & Profumo, S. 2014, ArXiv e-prints: 1408.1699
- Kalberla, P. M. W., Burton, W. B., Hartmann, D., et al. 2005, A&A, 440, 775
- Kuntz, K. D. & Snowden, S. L. 2000, ApJ, 543, 195
- Malyshev, D., Neronov, A., & Eckert, D. 2014, ArXiv e-prints: 1408.3531
- Million, E. T., Allen, S. W., Werner, N., & Taylor, G. B. 2010a, MNRAS, 405, 1624
- Million, E. T., Werner, N., Simionescu, A., et al. 2010b, MNRAS, 407, 2046
- Navarro, J. F., Frenk, C. S., & White, S. D. M. 1996, ApJ, 462, 563
- Riemer-Sorensen, S. 2014, ArXiv e-prints: 1405.7943
- Sanders, J. S. & Fabian, A. C. 2007, MNRAS, 381, 1381
- Sanders, J. S., Fabian, A. C., Churazov, E., et al. 2013, Science, 341, 1365
- Sidher, S. D., Sumner, T. J., Quenby, J. J., & Gambhir, M. 1996, A&A, 305, 308
- Simionescu, A., Allen, S. W., Mantz, A., et al. 2011, Science, 331, 1576
- Simionescu, A., Werner, N., Urban, O., et al. 2013, ApJ, 775, 4
- Smith, R. K., Brickhouse, N. S., Liedahl, D. A., & Raymond, J. C. 2001, ApJ, 556, L91
- Tamura, K., Ogasaka, Y., Naitou, M., et al. 2006, in Society of Photo-Optical Instrumentation Engineers (SPIE) Conference Series, Vol. 6266, Society of Photo-Optical Instrumentation Engineers (SPIE) Conference Series
- Tamura, T., Maeda, Y., Mitsuda, K., et al. 2009, ApJ, 705, L62
- Tawa, N., Hayashida, K., Nagai, M., et al. 2008, PASJ, 60, 11
- Urban, O., Simionescu, A., Werner, N., et al. 2014, MNRAS, 437, 3939
- Werner, N., Simionescu, A., Million, E. T., et al. 2010, MNRAS, 407, 2063
- Wright, C. O. & Brainerd, T. G. 2000, ApJ, 534, 34